SIMULATION OF EXPERIMENTS ON TRANSVERSE RMS-EMITTANCE GROWTH ALONG AN ALVAREZ DTL

L. Groening, W. Barth, W. Bayer, G. Clemente, L. Dahl,
P. Forck, P. Gerhard, I. Hofmann, G. Riehl, S. Yaramyshev, GSI, D-64291 Darmstadt, Germany
D. Jeon, SNS, ORNL, Oak Ridge, TN 37831, USA
D. Uriot, CEA IRFU, F-91191 Gif-sur-Yvette, France

Abstract

Systematic measurements on transverse rms-emittance growth along the Alvarez DTL of the GSI UNILAC were performed. A high intensity $^{40}Ar^{10+}$ beam was used to measure rms-growth for different transverse phase advances along the DTL. The transverse tune depression varied from 21% to 43%. For benchmarking of the experimental results three different beam dynamics codes were used: DYNAMION, PARMILA, and PARTRAN. This paper is on the results of the experiments, the reconstruction of the initial conditions for the simulations, and on the agreement between simulations and experiments. Additionally, successful suppression of rms-growth by systematic matching is reported.

INTRODUCTION

Transverse emittance growth is a major concern with respect to the preservation of beam quality during acceleration and transport along a linac beam line. In the last decades many beam dynamics computer codes were developed [1] in order to simulate the growth. Several benchmarking studies among codes have been performed, see for instance [2, 3, 4]. These studies generally assumed idealized conditions as initial Gaussian distributions, equal transverse emittances, matched injection into a periodic lattice, and small longitudinal emittance with respect to the rf-bucket size. In case of an operating linac most likely non of these conditions is met. In order to apply simulation codes to a more realistic environment a benchmark activity was started aiming at the simulations of systematic beam emittance measurements performed at an DTL entrance and exit, respectively. The studies were performed at the GSI UNILAC [5]. A more detailed description is given in [6].

For the simulations three different codes were used: DYNAMION [7], PARMILA (V 2.32) [8], and PARTRAN [9]. The first code uses 3D-particle-particle interaction of a few thousand particles and the other codes use PICNIC-3D Poisson solvers with some 10^5 particles. The rf-fields are calculated from the drift tube geometry for all codes. DYNAMION solves the Laplace Equation to generate the electric field on a grid followed by particle tracking. PARMILA and PARTRAN use tables of time transit factors generated by SUPERFISH to apply non-linear kicks to the particles.

EXPERIMENT SET-UP AND PROCEDURE

Intense beams are provided by MEVVA, MUCIS, or CHORDIS sources at low charge states with the energy of 2.2 keV/u. An RFQ followed by two IH-cavities (HSI section) accelerates the ions to 1.4 MeV/u using an rf-frequency of 36 MHz. A subsequent gas-stripper increases the average charge state of the ion beam. Final acceleration to 11.4 MeV/u is done in the Alvarez DTL section operated at 108 MHz. The increase of rf-frequency by a factor of three requires a dedicated matching section preceding the DTL. It comprises a 36 MHz buncher for longitudinal bunch compression, a 108 MHz buncher for final bunch rotation, a quadrupole doublet for transverse compression, and a quadrupole triplet for final transverse beam matching.

The Alvarez DTL comprises five independent rf-tanks. Transverse beam focusing is performed by quadrupoles in the F-D-D-F mode. Each drift tube houses one quadrupole. The periodicity of the lattice is interrupted by four inter-tank sections, where D-F-D focusing is applied. Acceleration is done -30° from crest in the first three tanks and -25° from crest in the last two tanks.

Figure 1 presents the schematic set-up of the experiments. A high current beam of $^{40}Ar^{1+}$ is delivered from

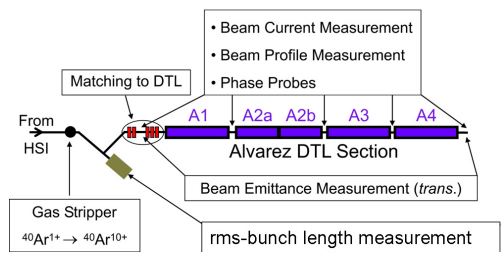

Figure 1: Schematic set-up of the experiments.

the HSI and passed through the gas stripper. A system composed of three dipoles and horizontal scrapers selects the desired charge state of 10+.

Beam current transformers are placed in front of and behind the DTL to measure the beam transmission. Horizontal and vertical slit/grid emittance measurement devices are located in front of and behind the DTL. The total accuracy of each rms-emittance measurement including its evaluation is estimated to be 10%. A set-up to measure the longitudinal rms-bunch length is available in front of the DTL [10]. It measures the time of impact of a single ion on

a foil. This time is related to a 36 MHz master oscillator. The resolution is 0.3° (36 MHz).

The HSI section was set to obtain 7.1 mA of $^{40}Ar^{10+}$ in front of the DTL (this current provides space charge equivalence to the UNILAC design beam of 15 mA of $^{238}U^{28+}$). Horizontal and vertical phase space distributions were measured in front of the DTL with a resolution of 0.8 mm in space and 0.5 mrad in angle. Additionally, the longitudinal rms-bunch length was measured at the entrance to the DTL. The DTL quadrupoles were set to zero current transverse phase advances σ_o ranging from 35° to 90° in steps of 5°. Due to space charge the phase advances in all three dimensions were depressed. The transverse depression reached from 21% (90°) to 43% (35°). After setting the desired σ_o along the DTL the quadrupoles and bunchers preceding the DTL were set to obtain full transmission through the DTL and to minimize low energy tails of the beam. For each value of σ_o horizontal and vertical beam emittances were measured at the exit of the DTL. In order to check the reproducibility of the measurements seven settings of σ_o were measured twice. The observed differences between two measurements using the same settings were just a few percent in rms-emittances. After the full σ_o scan the initial transverse emittances in front of the DTL were re-measured as well as the initial rms-bunch length.

DATA REDUCTION

Each emittance measurement delivers a two dimensional matrix of discrete slit-positions and discrete angles (in the following the term emittance refers to the phase space area divided by π). The data are processed by the measurement & evaluation program PROEMI [11]. Fractional emittances can be extracted as well since in practical cases it is beneficial to focus on the "inner" 95% of the particles. The emittance containing a given percentage p of the full distribution is extracted as follows: (i) The sum $\sum_{100}$ of all pixel contents is calculated. (ii) The pixels are sorted by their content starting from the largest one. (iii) Starting from the largest content the sum of all pixel contents is built as long as this sum is less or equal to the percentage p of $\sum_{100}$. (iv) Those pixels that contributed to the sum are considered for the rms-evaluation.

Simulations deliver a set of six dimensional particle coordinates. This ensemble is projected onto a pixel-grid having the same characteristics as the slit/grid device used for the measurements. The grid is read by the measurement evaluation program PROEMI such that data reduction was done in the same way as for measured data.

INPUT FOR SIMULATIONS

From the transverse emittances measured in front of the DTL normalized 100%-rms-emittances of 0.12 and 0.23 mm mrad were evaluated horizontally and vertically, respectively. Measuring the rms-bunch length in front of the DTL a value of 25 mm was found corresponding to a phase spread of 20° at 36 MHz.

The reconstruction of the initial distribution is done in two steps. First the 100%-rms-Twiss parameters are determined. In the second step the type of distribution is reconstructed. The transverse rms-measurements and the longitudinal rms-measurements on the initial distribution, done at different locations along the beam line (Fig. 2), had to be combined.

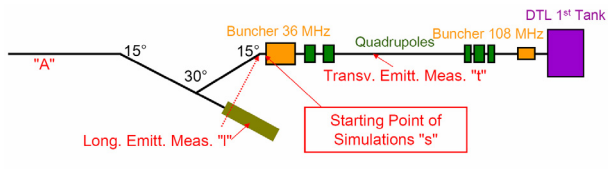

Figure 2: Reference points used for reconstruction of the initial phase space distribution.

This was achieved by attaching to the transverse rms-parameters measured at location "t" such longitudinal rms-parameters that result in the measured rms-bunch length measured at location "l", after rms-tracking the distribution from "t" to "s". The tracking implies the assumption that the virtual transport from "l" to "s" can be approximated by a simple drift including space charge. The length of this drift is given by the difference of the distances ("A", "l") and ("A", "s"), i.e. 0.4 m. Additionally, the recombined distribution must result in longitudinally matched injection into the DTL in accordance with the measurements. Eventual longitudinal mismatch could have been observed experimentally by transmission loss and the occurance of low energy tails. Applying this method the initial longitudinal 100%-rms-emittance was reconstructed as 22 deg mrad. The value refers to 36 MHz and to the relative momentum deviation.

Emittance growth depends on the kind of distribution, i.e. its halo. The amount of halo is estimated by evaluating the fractional rms-emittances and by plotting the fractional rms-emittance as function of the fraction. In case of a homogeneous distribution, i.e. no halo, the curve is just a straight line. For distributions with a halo the curvature of the graph is increased. The brilliance curve corresponding to the horizontal emittance measurement in front of the DTL is presented in Fig. 3. The horizontal brilliance curve of the initially measured distribution can be well reproduced by a Gaussian distribution cut at 4σ. Evaluating the vertical brilliance curve (Fig. 4) delivers an even stronger halo with respect to the horizontal projection of the initially measured distribution. Using a Gaussian cut at 4σ would underestimate the vertical halo significantly. In order to reproduce the brilliance curves in both transverse projections an appropriate six dimensional distribution function must be found. This was achieved using a distribution function as

$$f(R) = \frac{a}{2.5 \cdot 10^{-4} + R^{10}}, \quad R \leq 1 \qquad (1)$$

and $f(R)$=0 for $R > 0$ with

$$R^2 = X^2 + X'^2 + Y^{1.2} + Y'^{1.2} + \Phi^2 + (\delta P/P)^2 , \quad (2)$$

where a is the normalization constant and the constant in the demoninator results from the cut off condition at $R = 1$. By defining the radius R using different powers for different sub phase spaces the curvatures of the respective brilliance curves could be reproduced. Figures 3 and 4 plot the brilliance curves obtained from the distribution function f. The shape of the measured horizontal and vertical brilliance curve is reproduced very well, respectively.

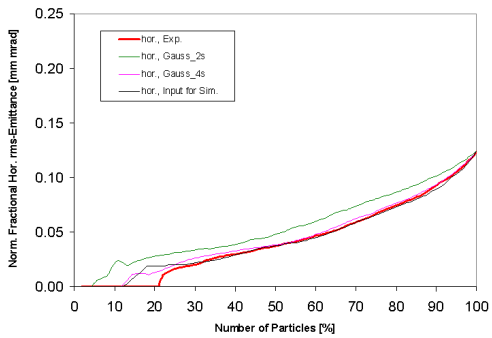

Figure 3: Brilliance curves of the horizontal phase space distribution in front of the DTL. The curves were extracted from the measured distribution (red bold), a Gaussian cut at 2σ (green), a Gaussian cut at 4σ (pink), and from the distribution used for the simulations (black).

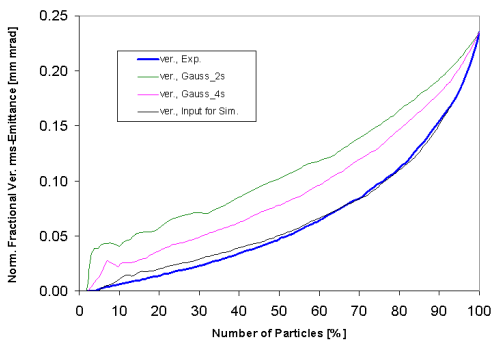

Figure 4: Brilliance curves of the vertical phase space distribution in front of the DTL. The curves were extracted from the measured distribution (blue bold), a Gaussian cut at 2σ (green), a Gaussian cut at 4σ (pink), and from the distribution used for the simulations (black).

Since for the longitudinal phase space distribution no measurement but on the rms-bunch length is available, a Gaussian distribution cut at 4σ is assumed. This can be achieved by setting the respective powers in the definition of R to a value of 2. Concerning the ambiguity on longitudinal input, simulations were performed using different types of longitudinal distributions. The final transverse emittances did effectively not change with the longitudinal distribution type.

The distribution reconstructed from f (Fig. 5) was used for simulations using DYNAMION (4300 particles), PARMILA, and PARTRAN. The last two codes used identical distributions of $2{\cdot}10^5$ particles.

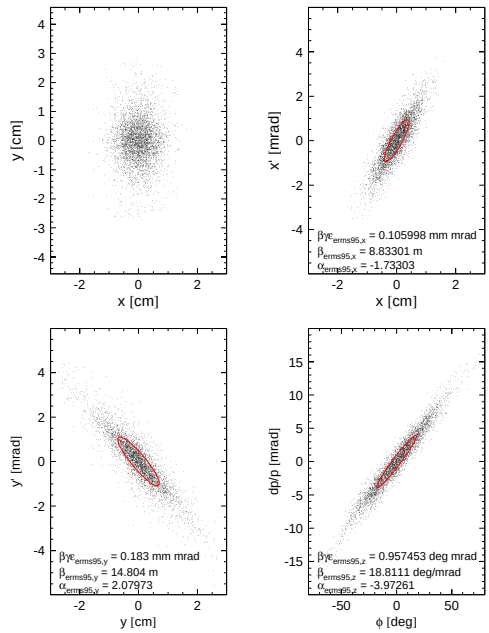

Figure 5: Initial distribution used for the DYNAMION simulations. 95%-rms-Twiss parameters are indicated. Phases refer to 36 MHz.

COMPARISON OF RESULTS

For all zero current phase advances σ_o ranging from 35° to 90° full beam transmission was observed through the DTL in the experiment. All simulations codes revealed losses of about 2%. Figure 6 shows final horizontal phase space distributions at the DTL output as obtained from the measurements and from the simulations for three different values of σ_o. For all σ_o the simulations delivered final phase space distributions with elliptical symmetry. Just at highest phase advances two symmetric wings attached to the core are observed in the horizontal distributions. This is in agreement with the measurements. The measured distributions for very low and very high σ_o gave inhomogeneous shapes as seen for the σ_o = 35° case at the left of Fig. 6. Generally, the simulated shapes look quite similar for all codes.

The shapes of longitudinal distributions at different locations along the DTL from simulations depend weakly on the transverse phase advance. Filamentation occurs due to the large initial longitudinal emittance.

Transverse 95%-rms-emittances at the exit of the DTL are plotted in Figs. 7 to 9 as function of the zero current phase advance σ_o along the DTL. Generally lowest growth rates were found for phase advances close to 60° experimentally and in simulations. However, scattering of the individual values around this general behaviour is found.

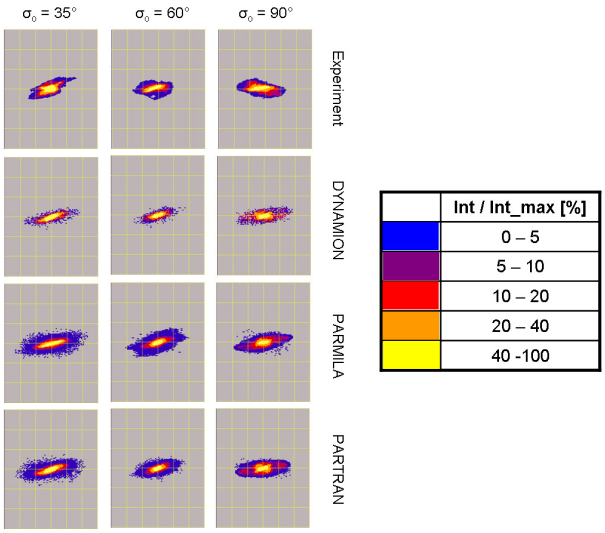

Figure 6: Top to buttom: horizontal phase space distributions at the DTL exit. Left: σ_o = 35°; centre: σ_o = 60°; right: σ_o = 90°. The scaling is $\pm$ 24 mm (horizontal axis) and $\pm$ 24 mrad (vertical axis), respectively.

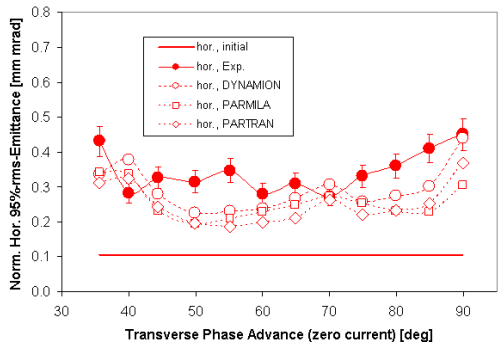

Figure 7: Horizontal 95%-rms-emittance at the end of the DTL as function of σ_o.

The codes predict very similar dependence of the horizontal and vertical growth on σ_o, i.e. a minimum at intermediate phase advances and significant growth for very low and very high phase advances. This behaviour is in agreement with the measurements.

In the vertical plane (Fig. 8) high growth rates were measured for the lowest phase advances of 35° and 40° exceeding the rates measured horizontally. This behaviour was not reproduced by any of the simulation codes. The codes rather predict weak dependence on the phase advance for $\sigma_o \leq 60°$. For higher phase advances a slight increase of the growth was measured while the codes predict stronger growth. As already observed in the horizontal plane the codes produce similar dependence of the vertical emittance growth on σ_o. The resulting rms-emittances of the codes differ just slightly from each other. For $\sigma_o \geq 50°$ the emittances from the codes agree with the measurements within the error bars. For high phase advances the difference among the codes are largest.

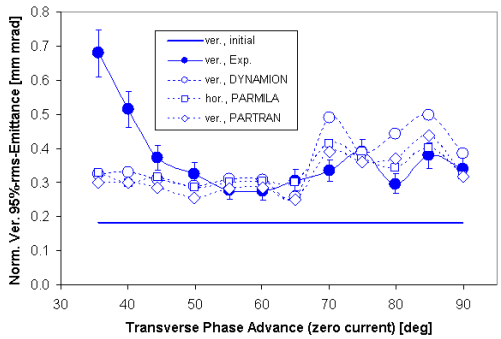

Figure 8: Vertical 95%-rms-emittance at the end of the DTL as function of σ_o.

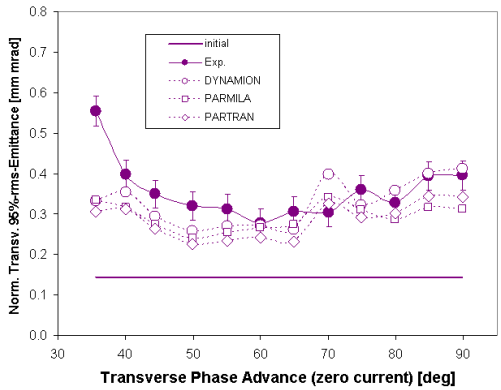

Figure 9: Mean value of horizontal and vertical 95%-rms-emittance at the end of the DTL as function of σ_o.

Evaluating the mean values of horizontal and vertical emittances (Fig. 9) results in a smoother behaviour with respect to the behaviour in the single planes. In the measurements a broad mimimum of the rms-emittance growth is found at $\sigma_o \approx 60°$. The scatter arround this general behaviour is reduced with respect to the scatter observed in the single planes. The codes reproduce the measured values within the error bars.

It might be argued if the observed differences of measured and simulated emittances is due to a wrong assumption on the initial longitudinal emittance. Simulations have been performed using initial longitudinal emittances of 2.3, 12, and 37 deg mrad (36 MHz) for the 45° case. The final transverse rms-emittances differed by 5% at maximum. The simulations assume a machine without any errors. Such errors generally drive additional emittance growth [12].

The amount of mismatch M was estimated using DYNAMION simulations by evaluating the simulated phase space distributions at the entrance to the DTL and comparing their rms-Twiss parameters with the periodic DTL solutions. M is calculated using the definition given in [13] and it is plotted as function of σ_o in Fig. 10. It turned out that the transverse mismatch varied with the phase advance.

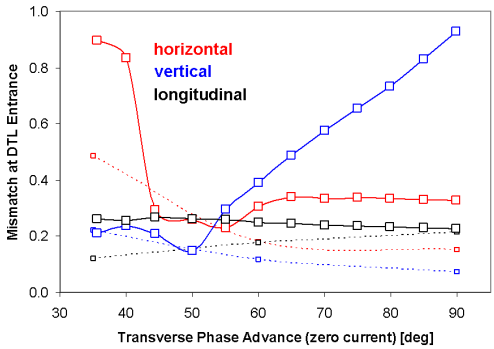

Figure 10: Mismatch between beam 95%-rms-Twiss parameters and periodic Twiss parameters at injection into the DTL as function of the phase advance σ_o for the benchmarking campaign (full) and the measurements with reduced mismatch (dashed).

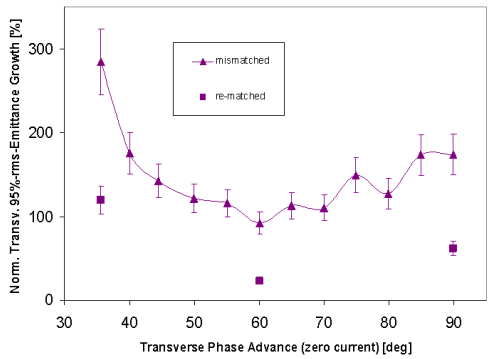

Figure 11: Growth of the mean value of horizontal and vertical 95%-rms-emittance along the DTL as function of the zero current phase advance σ_o.

REDUCTION OF MISMATCH AND EMITTANCE GROWTH

Using the reconstructed initial distribution as input for a dedicated rms-matching routine with space charge [14] is expected to lead to improved matching conditions. Ten months after the benchmarking campaign a $^{40}Ar^{10+}$ beam of 7.1 mA was used to re-measure transverse emittances in front of and behind the DTL for zero current phase advances of 35°, 60°, and 90°. Rms-matching with space charge was done using the reconstructed initial distribution. Using the DYNAMION code the remaining mismatch was estimated and is plotted in Fig. 10. The mismatch was strongly reduced with respect to the benchmarking.

During the later measurements two neighboring quadrupole lenses in tank A3 of the DTL had to be switched off due to cooling water leakage. In order to avoid mismatch in connection with longitudinal focusing, the rf-power in tanks A3 and A4 was switched off. Transverse rms-emittances were measured after tank A4. The emittance growth along the DTL tanks that are not rf-powered (A3, A4) can be neglected with respect to the growth along rf-powerd DTL tanks. This assumption was verified in simulations and experimentally [15]. The measured rms-emittance growth rates are plotted in Fig. 11 together with the corresponding values of the benchmarking campaign. It could be demonstrated that emittance growth is strongly driven by rms-mismatch and that rms-matching significantly reduced the transverse rms-emittance growth. These measurements confirmed that a valid procedure was applied during the benchmarking to reconstruct initial Twiss parameters.

ACKNOWLEDGEMENT

We acknowledge the support of the European Community-Research Infrastructure Activity under the FP6 “Structuring the European Research Area” programme (CARE, contract number RII3-CT-2003-506395).

The participation of D. Jeon to this work was made possible partly by the support of ORNL/SNS (managed by UT-Battelle, LLC, for the U.S. Department of Energy under contract DE-AC05-00OR22725).

REFERENCES

[1] R. Ryne et al., these proceedings.

[2] S. Nath et al., Proc. of the 2001 Part. Accel. Conf., Chicago, U.S.A., (2001).

[3] A. Franchi et al., Proc. of the XXIII Linac Conf., Knoxville, U.S.A., (2006).

[4] A. Franchi et al., http://www-dapnia.cea.fr/Phocea/file.php?class=std&&file=Doc/Care/note-2006-011-HIPPI.pdf

[5] W. Barth et al., Proc. of the XXII Linac Conf., Lübeck, Germany, (2004).

[6] L. Groening et al., Phys. Rev. ST Accel. Beams **11**, 094201 (2008).

[7] S. Yaramyshev et al., Nucl. Instrum. & Methods in Phys. Res. A **558**, 1, (2006).

[8] J.H. Billen and H. Takeda, PARMILA Manual, Report LAUR-98-4478, Los Alamos, 1998 (Revised 2004).

[9] R. Duperrier et al., ICSS 2002 Conf., Amsterdam, The Netherlands (2002).

[10] P. Forck et al., Proc. of the XX Linac Conf., Monterey, U.S.A., (2000).

[11] G. Riehl, *PROEMI: An emittance measurement and evaluation code.* The manual is available from the code author on request (g.riehl@gsi.de).

[12] K.R. Crandall, AOT Division Technical Note LA-CP-96-16, January 22, 1966.

[13] T.P. Wangler, “Rf Linear Accelerators”, John Wiley & Sons Inc., New York, p. 217, (1998).

[14] L. Groening, http://www-linux.gsi.de/∼lgroenin/bd_unilac/HSI/Alvarez_Matching.html.

[15] L. Groening et al., http://www-dapnia.cea.fr/Phocea/file.php?class=std&&file=Doc/Care/care-report-07-030.pdf